Measurement Science
and Technology

100 year anniversary
Measurement Science and Technology

PURPOSE-LED
PUBLISHING™

PAPER • **OPEN ACCESS**

Non-intrusive torque measurement for rotating shafts using optical sensing of zebra-tapes

To cite this article: D Zappalá *et al* 2018 *Meas. Sci. Technol.* **29** 065207

View the article online for updates and enhancements.

You may also like

- Dynamic torsional response analysis of mechanoluminescent paint and its application to non-contacting automotive torque transducers
Gi-Woo Kim and Ji-Sik Kim
- A self-calibrating multicomponent force/torque measuring system
Rafael R Marangoni, Jan Schleichert, Ilko Rahneberg et al.
- Design and Research of High Precision Dynamic Torque Measurement System
Yang Su, Lei Cheng and Lifang Wang

This content was downloaded from IP address 220.203.226.175 on 20/08/2025 at 02:24

OPEN ACCESS
IOP Publishing
Measurement Science and Technology
Meas. Sci. Technol. **29** (2018) 065207 (18pp)
https://doi.org/10.1088/1361-6501/aab74a

Non-intrusive torque measurement for rotating shafts using optical sensing of zebra-tapes

D Zappalá[1], M Bezziccheri[2], C J Crabtree[1] and N Paone[2]

[1] Department of Engineering, Durham University, Durham, United Kingdom
[2] Università Politecnica delle Marche, DIISM, Ancona, Italy

E-mail: donatella.zappala@durham.ac.uk

Received 22 May 2017, revised 13 March 2018
Accepted for publication 16 March 2018
Published 10 May 2018

Abstract

Non-intrusive, reliable and precise torque measurement is critical to dynamic performance monitoring, control and condition monitoring of rotating mechanical systems. This paper presents a novel, contactless torque measurement system consisting of two shaft-mounted zebra tapes and two optical sensors mounted on stationary rigid supports. Unlike conventional torque measurement methods, the proposed system does not require costly embedded sensors or shaft-mounted electronics. Moreover, its non-intrusive nature, adaptable design, simple installation and low cost make it suitable for a large variety of advanced engineering applications. Torque measurement is achieved by estimating the shaft twist angle through analysis of zebra tape pulse train time shifts. This paper presents and compares two signal processing methods for torque measurement: rising edge detection and cross-correlation. The performance of the proposed system has been proven experimentally under both static and variable conditions and both processing approaches show good agreement with reference measurements from an in-line, invasive torque transducer. Measurement uncertainty has been estimated according to the ISO GUM (Guide to the expression of uncertainty in measurement). Type A analysis of experimental data has provided an expanded uncertainty relative to the system full-scale torque of $\pm 0.30\%$ and $\pm 0.86\%$ for the rising edge and cross-correlation approaches, respectively. Statistical simulations performed by the Monte Carlo method have provided, in the worst case, an expanded uncertainty of $\pm 1.19\%$.

Keywords: non-intrusive torque measurement, zebra tape, pulse train time shift, shaft twist angle, pulse train rising edge, cross-correlation, uncertainty

(Some figures may appear in colour only in the online journal)

1. Introduction

Torque is a fundamental operating parameter of rotating mechanical systems. Some of the most common industrial applications of torque measurement include both conventional [1, 2] and emerging [3, 4] power generation, electric motor testing [5], robot arms [6], marine [7] and automotive [8] industry. Power and efficiency optimisation based on highly accurate and reliable torque measurement, besides enabling significant energy savings, fits to the steadily increasing requirements of the international regulation, especially for large mechanical drives with high nominal torque [9], such as marine engines [10]. Despite torque measurement and control being critical to dynamic performance monitoring, condition monitoring for predictive maintenance and control of mechanical systems, reliable measurements can be difficult to obtain in a cost-effective and non-intrusive manner.

Original content from this work may be used under the terms of the Creative Commons Attribution 3.0 licence. Any further distribution of this work must maintain attribution to the author(s) and the title of the work, journal citation and DOI.

The methods used to measure torque can be divided into two categories, either direct or indirect.

Direct methods use in-line torque transducers, already calibrated by the manufacturer, which are integrated into the drive shaft. These sensors have some susceptibility to noise and require bearings for support, which also implies maintenance. The major obstacle to the industrial application of direct measurement systems is the costly and intrusive nature of the required equipment, which is impractical for short-term use, particularly on large systems. The act of mounting the in-line transducer may also change system dynamics and, consequently, torque values. Moreover, direct measurements cannot be implemented when the rotating mechanical system design does not allow adapting the shaft design or lengthening the drivetrain to accommodate the in-line transducer.

Indirect methods are based on the measurement of torque-related parameters and subsequent torque calculation. These methods have the advantage of avoiding modifications to the original shaft, therefore minimising the impact on mechanical design and not modifying the static and dynamic behaviour of the shaft. The conventional indirect systems are based on measurement of surface strain or angle of twist [11]. Surface strain measurement systems typically use either strain gauges, directly bonded on the shaft body in a Wheatstone bridge configuration, or magnetostrictive methods. These methods rely on the change of resistance [12] or magnetization properties of the material [13], respectively, when torque is applied. Strain gauges are the most commonly used in industrial applications thanks to their low cost and high sensitivity. However, the main limitations of this method are the complexity of installation of the sensors on cylindrical surfaces, the need to install electronics on the rotating shaft, the requirement for specialised personnel required for installation, usability, resolution, noise susceptibility and the requirement for regular calibration. Moreover, unwanted forces can create unintended directional disturbance, such as crosstalk phenomena, that can increase the uncertainty in the measured loads and reduce accuracy [13]. Angle of twist measurement methods are based on the measurement of the phase between two points on the shaft, separated by a suitable distance, through magnetic or optical angular position sensing [7]. The first use toothed gears which are angularly displaced with respect to each other as the shaft shift twist angle increases, thereby increasing the electrical phase difference between the signals measured by magnetic pickups [13]. Conventional optical methods use slotted discs which move with respect to each other as torque is applied, thereby changing the on-times of light pulses created by the shutter actions of the rotating discs [14, 15]. Both systems can be retrofitted to existing systems and do not have the inherent complexity of strain gauge installations. However, they require the installation of quite large rings and plates around the shaft which can be impractical in some industrial applications, such as in-vehicle and mobile measurements, due to space constraints. They also suffer from environmental factors such as dust, humidity, temperature, vibration, electromagnetic interference and aging. In addition to performance limitations, these methods usually suffer from low range-to-resolution ratio [11]. A laser torque meter was first presented in [16] and later analysed in [17–19]. This instrument is based on the cross-correlation of the periodic speckle patterns generated by two axially separated laser beams on a rotating shaft, having known mechanical proprieties. Even if this is a smart non-contact approach, it suffers from decorrelation of speckle patterns due to shaft displacement and tilt, making its practical application difficult. Several advanced contactless torque measurements techniques have been researched recently, such as the photo-elastic torque sensor based on the birefringence effect of optically anisotropic materials [20] and the non-contact Hall effect design sensor [21]. However, most of these sensors have significant limitations such as requiring torque sensitive materials to be attached on the shaft surface, such as ferromagnetic and piezoelectric materials, and limited speed range and resolution. Moreover, very few solutions can provide both shaft torque and speed measurement from the same sensor, which is useful whenever one desires to measure mechanical power.

This paper presents a novel and simple contactless torque and speed measurement system consisting of two zebra tape codes directly glued around the shaft with two optical sensors mounted on non-rotating supports. This technique operates entirely contact-free and allows torque measurement on standard installations, across their operational life, avoiding the use of permanently installed in-line intrusive torque meters, by simply instrumenting the existing shaft with the two zebra tapes located as far as possible from each other. The use of optical sensors and zebra tapes on rotating shafts is not new; however, literature reports only application for torsional vibration measurement [22, 23], while this research proposes their use for torque measurement. This paper introduces the operating principle of the proposed non-intrusive torque measurement system and its experimental implementation and validation. Two different approaches for processing the optical probe (OP) pulse train signals and estimating the shaft twist, and hence the applied torque, are then presented. After calibrating the system under stationary conditions, its response and performance under both static and time-varying torque conditions is demonstrated by comparing the results of the two proposed signal processing approaches against the reference measurements from an in-line torque transducer mounted on the test bench shaft.

2. Methodological approach

A torque acting on a shaft causes the shaft itself to twist, with one end rotating with respect to the other by an angle displacement θ. Assuming a uniform circular cross-section and linear homogenous elastic material, the relationship between the torque applied to a rotating shaft, T (N m), and the relative rotation of the ends of the shaft section, θ (rad), is described [24] by:

$$T = I\ddot{\theta} + C\dot{\theta} + K\theta \tag{1}$$

where I is the rotating system moment of inertia (kg m^2), C is the shaft damping coefficient (kg m^2 s^{-1} rad^{-1}) and K is the shaft torsional stiffness (N m rad^{-1}).

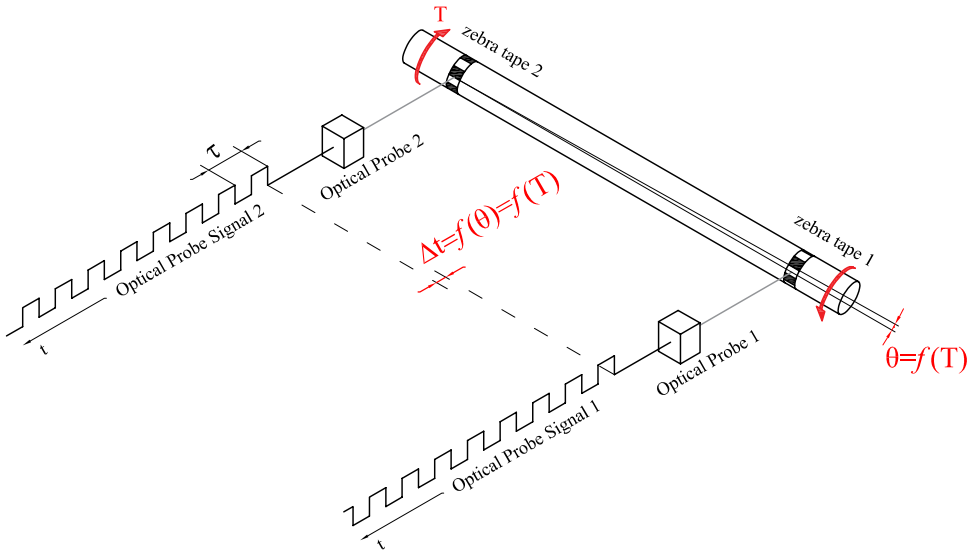

Figure 1. Operating principle of the non-intrusive torque measurement system.

The non-intrusive torque measurement system proposed in this paper employs a set of two zebra tapes and two OPs, one at each end of the shaft, as shown in figure 1.

The zebra tapes feature an equal number of equidistant black and white stripes and are glued around the shaft. As the shaft rotates, each optical sensor, mounted on a non-rotating component, generates a pulse train signal proportional to the light intensity reflected by the zebra tape stripes. When a torque, T, is applied to the shaft, the relative rotation of the ends of the shaft section, θ, results in a time shift, Δt, between the two pulse train signals. The principle of the proposed method is to quantify the shaft relative twist angle by measuring the phase difference between the two pulse signals and thence deriving the applied torque, from a known torque-twist relationship. This is achieved according to the following procedure:

(1) Estimation of the time shift, Δt (s), between the pulse trains measured by the two OPs;
(2) Measurement of the pulse trains period, τ (s), and calculation of the shaft rotational speed, n (rpm):

$$n = \frac{60}{\tau\, ppr} \tag{2}$$

where ppr is the number of pulses per shaft revolution;
(3) Conversion of time shift to absolute angular shift, θ_a, according to [25]:

$$\theta_a = \frac{2\pi}{60} n \Delta t. \tag{3}$$

The shaft absolute twist angle, θ_a, could be different to the shaft relative twist angle, θ, due to the mounting misalignment between the two OPs and/or the two zebra tapes. This error manifests itself as an apparent angular shift, $\theta_{a,0}$, at the no load condition;

(4) Calculation of the shaft relative twist angle, θ, according to the following equation:

$$\theta = \theta_a - \theta_{a,0}. \tag{4}$$

(5) Estimation of the shaft torque based on the known calibration curve, that is the relationship between the shaft relative twist angle θ and torque T for a given shaft and material.

One of the main advantages of this approach is that it allows the measurement of a wide torque range by carefully designing the zebra tapes and their distance along the shaft. This makes it suitable for a large variety of engineering applications.

3. Experimental set-up

Experiments were performed to calibrate and validate the proposed non-intrusive torque measurement system. The calibration was performed by comparing the zebra tape torque meter with a reference state-of-the-art measurement technique; in particular, an industrial in-line torque meter, based on the principle of a variable, torque-proportional transformer coupling, was used. This technology is robust against electromagnetic interference and temperature effects; therefore, the system can be effectively used as a reference for calibration. Figure 2 provides a schematic of the torque test rig developed at Durham University, in collaboration with Università Politecnica delle Marche. Figure 3 shows the implemented test stand with its main components and instrumentation.

The test rig comprises a 4-pole 4 kW grid-connected induction generator driven by a 4-pole 4 kW induction motor controlling the speed profile. Both machines are manufactured by ABB Motors. The motor shaft speed is varied via an inverter drive up to 2100 rpm. The generator is connected to a variable transformer to vary its stator voltage and hence the shaft torque in the range from 0 to 16 N m.

The main rig solid shaft, shown schematically in figure 4, features a reduced diameter cross-section in its central part for experimental purposes in order to enhance sensitivity

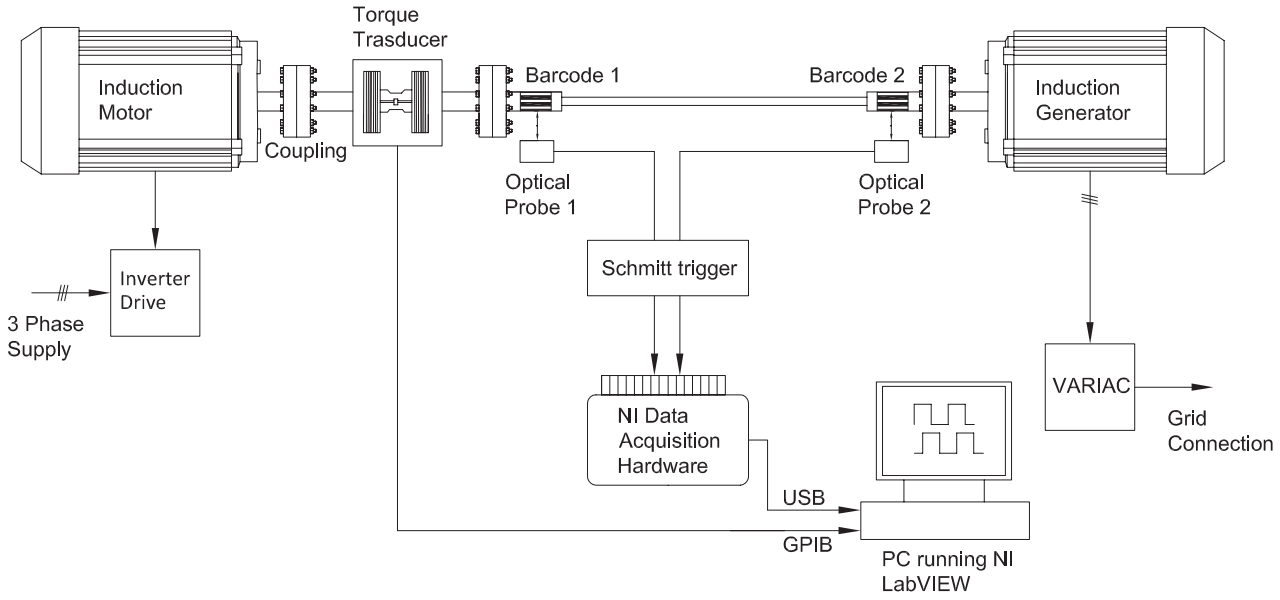

Figure 2. Schematic diagram of the torque test rig.

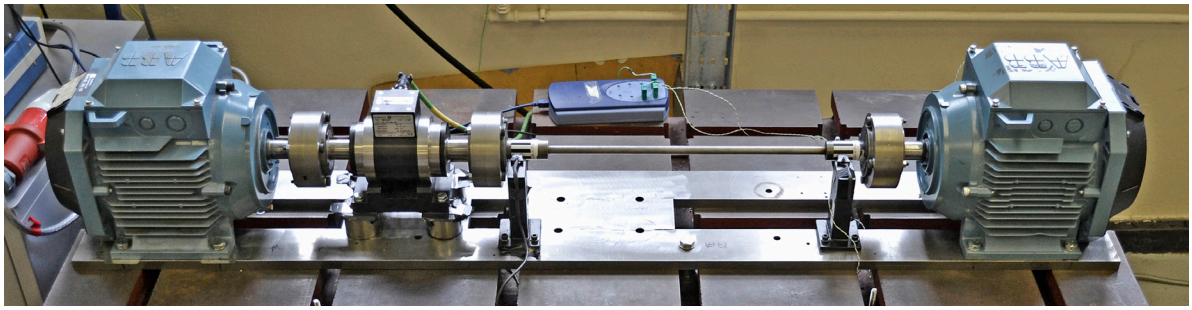

Figure 3. Main components and instrumentation of the torque test rig.

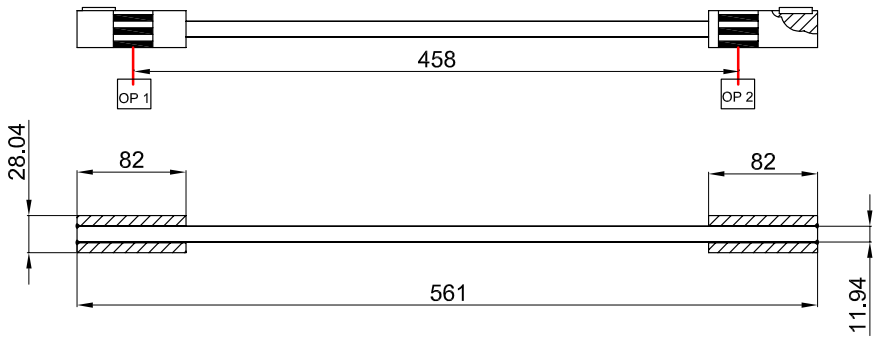

Figure 4. Solid shaft layout and location of the two zebra tapes.

with respect to the test rig torque range and hence achieve a higher twist angle θ for the same applied torque. Indeed, this allows angular shifts of the same order of magnitude as would be observed in the case of larger torques applied to larger diameter shafts in industrial applications, despite the limitations of the maximum torque possible using this test rig.

A high-quality, laser-printed zebra tape is glued around each end of the shaft. The passage of the alternating light and dark stripes is measured by two Optek OPB739RWZ reflective line reader sensors placed at the optimum distance of 0.76 mm from the target, as shown in figure 5.

First, the output from the two OPs is transformed into a series of square pulses through a Schmitt trigger. The pulses are then acquired by a National Instruments (NI) 16-bit data acquisition system (USB-6211 DAQ) driven by the LabVIEW data acquisition environment. The sampling frequency, f_{OP}, is set at 125 kHz, the maximum possible for the NI USB-6211 DAQ hardware.

An in-line Magtrol TMB 313/431 torque transducer, with a rated torque of 500 N m and a combined error of linearity and hysteresis less than $\pm 0.15\%$ of the rated torque, acts as a reference for calibration and comparison with the optical non-intrusive system output. The transducer is capable of

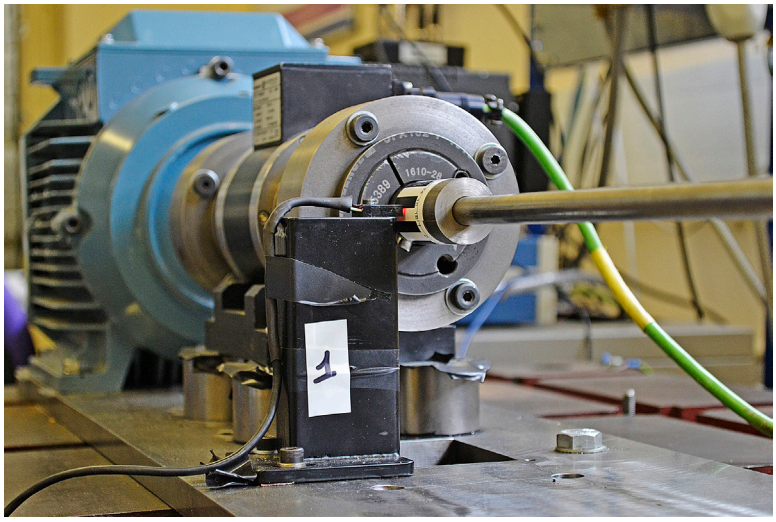

Figure 5. Detail of the contactless shaft torque measurement system.

outputting 60 pulses per revolution for speed measurement so is also used as a reference tachometer. The torque transducer output is collected through a Magtrol 6400 torque display which is connected by a GPIB/IEEE-488 interface to the LabVIEW data acquisition environment. The time synchronisation between the torque transducer and the OPs' readings is obtained by comparing the Unix timestamp of the two system acquisitions.

3.1. Zebra tape design

The design of the zebra tape, particularly the number of pulses per revolution, has a significant impact on the precision of the torque measurements [26]. For a given shaft and zebra tape design, the maximum measurable phase difference between two pulse signals is given by half the zebra tape period, that is half the length of each of its black–white segments, corresponding to 180° phase shift. Indeed, any twist larger than half the period of the zebra tape would be confused with a lower one, as always happens in periodic signals.

When designing the zebra tapes, the minimum zebra tape period, $P_{\min}$ (m), can be calculated as a function of the maximum torsion angle of the shaft expected during operation, $\theta_{\max}$:

$$P_{\min} > 2\theta_{\max} r \tag{5}$$

where $\theta_{\max}$, (rad) is given by:

$$\theta_{\max} = \frac{T_{\max} L}{JG} \tag{6}$$

where $T_{\max}$ is the maximum torque expected during operation (N m), L is the distance between the two OPs (m), J is the shaft polar moment of inertia (m^4) and G is the shear modulus of elasticity for the shaft material (Pa). The corresponding zebra tape maximum allowable number of pulses per revolution, $ppr_{\max}$, can then be calculated as:

$$ppr_{\max} = \text{int}\left(\frac{2\pi r}{P_{\min}}\right) < \frac{2\pi r}{2\theta_{\max} r} \tag{7}$$

where r (m) is the shaft radius and int the integer part function.

Table 1. Features of the experimental zebra tape.

Symbol	Description	Value
P	Zebra tape period (length of each black–white segment)	11.0 mm
ppr	Number of pulses per revolution	8
$\theta_{\text{full\_scale}}$	Maximum measurable shaft torsion angle	$\frac{\pi}{8}$

In the case of the experimental test bench described in this work, given the shaft geometry and the maximum torque achievable during operation (16 N m) equation (7) provides a maximum allowable number of pulses per revolution of 45. Within this constraint, the choice of the zebra tape design is a key factor influencing the performance of the proposed torque measurement system. The larger the number of pulses per revolution, the larger the samples required per revolution, that is the larger the sample frequency of the proposed torque transducer, but the more the computational cost needed to implement the data processing. For the purpose of this work, the test bench shaft was instrumented with two bar codes featuring 8 equal stripe pairs, with a stripe width of 5.5 mm, fitting exactly around the shaft. The selection of 8 pulses per revolution represents a trade-off between uncertainty and computational cost. The zebra tape design was selected so that the resulting pulses have a 50% duty cycle which makes phase shift measurement processing easier.

Table 1 summarises the features of the zebra tapes used in the test bench.

3.2. Optical sensor output

Figure 6(a) shows how the zebra tape passage determines the sensor output. The OP emits an unfocussed beam which lights the zebra tape surface. An unfocussed OP has been chosen because it allows for variations of sensor to shaft distance over a larger depth of field with respect to focused probes. However, it produces pulses with lower rising and falling edge gradients, with respect to focused probes. Scattered

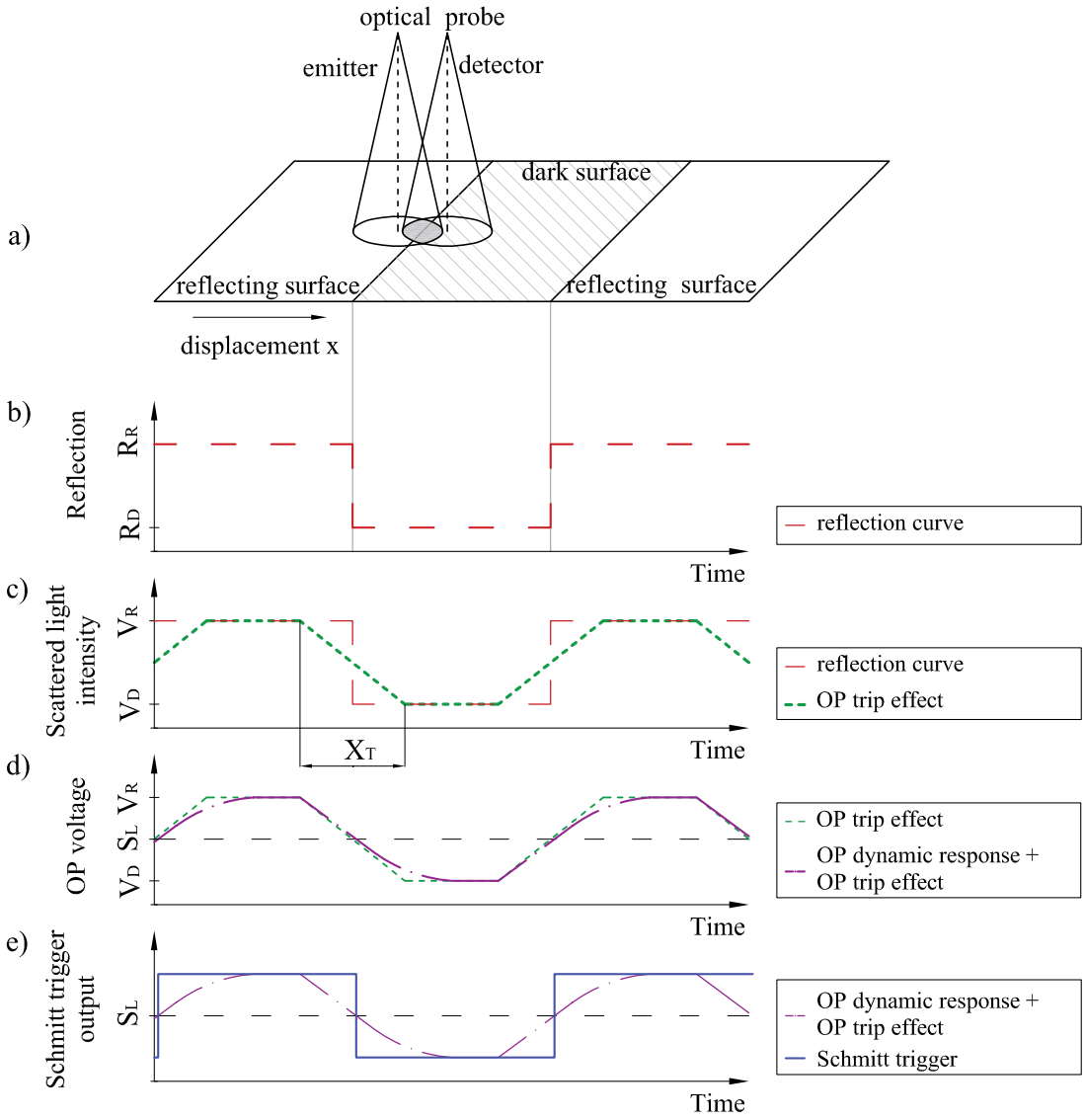

Figure 6. OP response to zebra tape. (a) Passage of the alternating reflecting and dark stripes measured by the OP sensor; (b) zebra tape step profile reflection; (c) scattered light intensity; (d) OP voltage output; (e) Schmitt trigger output.

light is collected back through a detector with a certain angle of aperture. Light scattering intensity from the white surface is significantly larger than that from the black surface. Therefore, even if the zebra tape surface has a step profile (figure 6(b)), the scattered light intensity changes continuously from low to high during the passage of the white stripe. The change in the radiation reflected to the detector is not abrupt, but undergoes a gradual transition along a switching distance X_T (figure 6(c)) [27]. The OP voltage output results from this gradual change in scattered light intensity due to the motion of the black–white stripe through the illuminated area (called trip effect) and the first order dynamic response of the photodetector (figure 6(d)). A Schmitt trigger is implemented to square the probe output voltage when it crosses a pre-set threshold, S_L (figure 6(e)), and to convert it into a train of constant amplitude pulses. The photodetector signal is squared to produce pulses with almost vertical rising and falling edges, easing timing and analysis.

This train of square pulses will be phase shifted by torque variations, as described earlier. In case of variation of the distance between the shaft and the OPs, the amplitude of the output voltage from the photodetectors will vary, resulting in an amplitude modulated signal. This would affect the train of pulses from the Schmidt trigger, which operates on a fixed threshold. The effects of this source of uncertainty will be discussed later in the paper.

3.3. Data processing

3.3.1. Signal pre-processing. In order to automatically extract the values of the shaft angular shifts from the two zebra tape optical signals, dedicated programmes, known as virtual instruments (VIs), were developed and built in the LabVIEW environment. Figure 7 shows the data processing flow chart of the VIs implemented for pulse train analysis.

The data processing consists of two steps:

(1) The shaft rotational speed is calculated by estimating the time per shaft revolution from the rising edges of the two pulse trains;

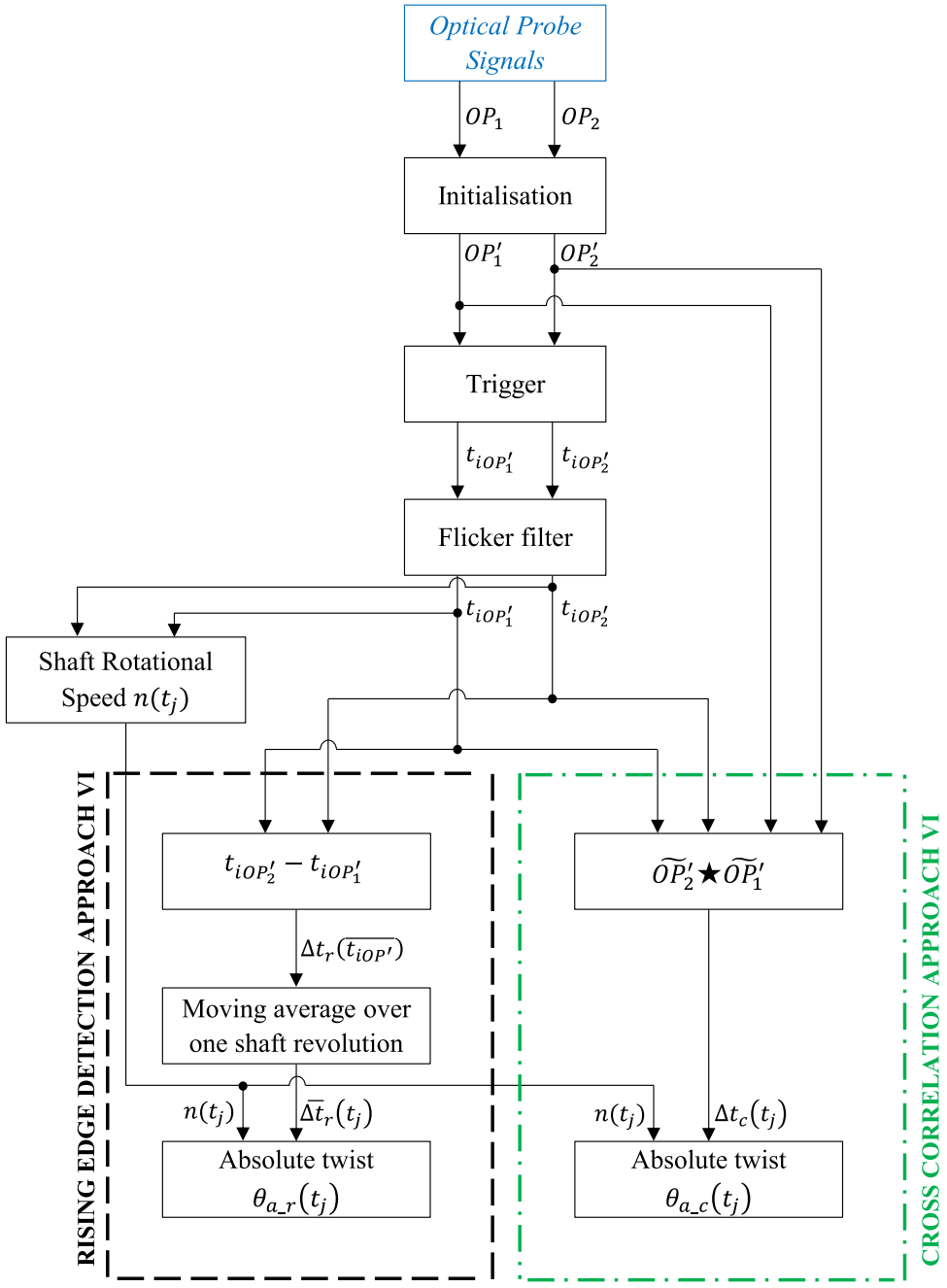

Figure 7. Data processing flow diagram.

(2) The shaft absolute twist is calculated by adopting the rising edge detection and the cross-correlation approaches.

OP installation and zebra tape mounting offset could cause initial misalignment of the pulse trains at the start of recording with a consequent erroneous estimation of the initial time shift, and hence angular shift. To overcome this problem, the signals recorded by the OPs are first initialised when the data system acquisition is started. Figures 8(a) and (b) shows an example of two pairs of similar pulse trains; they feature the same time shift, Δt_r, however their recording starts at two different positions with respect to the pulses. The time shift measured between their first two rising edges will be different, Δt_{r_a} and Δt_{r_b}, respectively. In order to avoid this error in the measurements, the OP signals, OP_1 and OP_2, are initialised by forcing the recording to start only when both signals are in the high or low state, i.e. at the instant t_p in figures 8(c) and (d). Now, the same time shift, Δt_r, is measured based on the time between the first rising edges of the initialised signals, OP'_1 and OP'_2.

The time at which the rising edges of the two initialized signals occur is defined as $t_{iOP'_k}$, where $i = 1,2, \ldots m$, with m equal to the number of rising edges in the initialized signals, and $k = 1,2$ is the index that identifies the two OPs. The rising edge time instants $t_{iOP'_k}$ are captured by triggered acquisition where the threshold level is set equal to half of the peak-to-peak signal amplitude. A flicker filter is also applied to remove rising edge timing errors resulting from possible signal flickering around the trigger level. Flickering would result in more

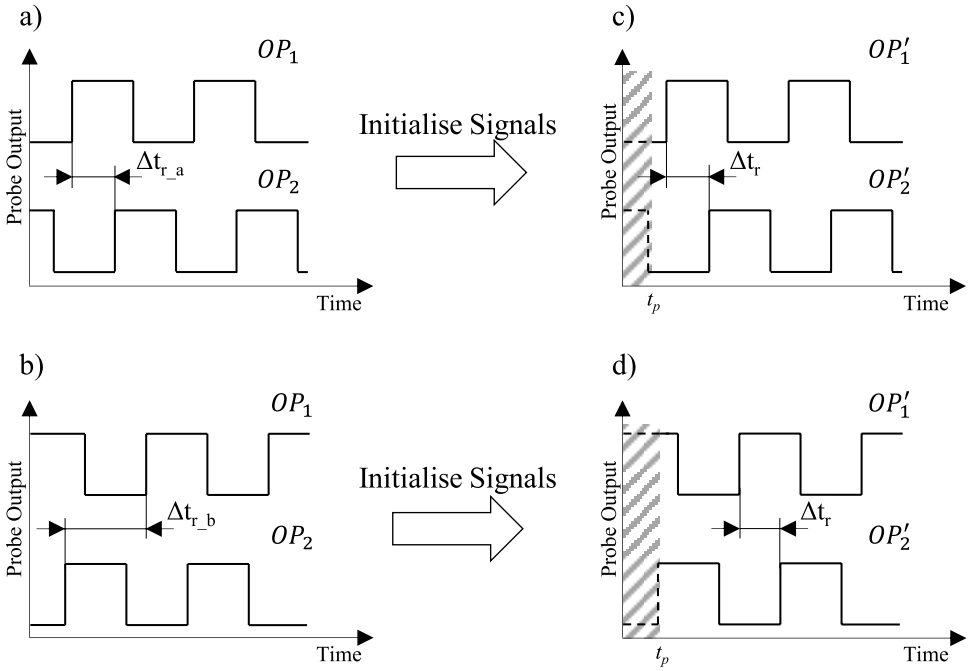

Figure 8. Signal initialisation (a) and (b) similar pulse trains recorded at two different start positions with respect to the pulse state; (c) and (d) OP initialisation with signals both in the high or low state.

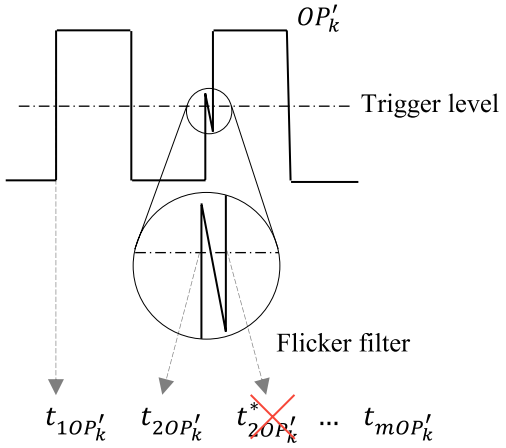

Figure 9. Flicker filter.

than one output from the trigger block for each signal rising edge, i.e. $t_{2\mathrm{OP}'_k}$ and $t^*_{2\mathrm{OP}'_k}$ in figure 9. For each pulse train, the filter compares the time interval between two consecutive rising edges against that estimated from the expected shaft rotational speed, 1500–1900 rpm, and the number of pulses per revolution, 8. When the two values do not match, the filter acts on the signal to keep only the first output from the trigger block and remove all other unwanted outputs, that is $t^*_{2\mathrm{OP}'_k}$ in figure 9. For each signal, the output of the flicker filter is a 1D array containing m elements representing the rising edge times of the train of pulses.

3.3.2. Shaft rotational speed. For each zebra tape, the identified rising edge times, $t_{i\mathrm{OP}'_k}$, where $k = 1,2$, are then used to estimate the corresponding shaft speed, $n_k\,(t_{k,j})$ (rpm), by applying conventional speed encoder techniques, according to equation (3), as follows:

$$n_k\,(t_{k,j}) = \frac{60}{t_{(ppr+l-1)\mathrm{OP}'_k} - t_{l\mathrm{OP}'_k}} \tag{8}$$

where $l = 1,2,..,\,(m\text{-}ppr)$ and $t_{k,j}$ is the mean time of the windows $t_{(ppr+l-1)\mathrm{OP}'_k} - t_{l\mathrm{OP}'_k}$, calculated as:

$$t_{k,j} = \frac{\sum_{n=j+1-\left|\frac{ppr}{2}\right|_{\mathrm{up}}}^{j+\left|\frac{ppr}{2}\right|_{\mathrm{down}}} t_{n\mathrm{OP}'_k}}{ppr} \tag{9}$$

where $j = \left(\left|\frac{ppr}{2}\right|_{\mathrm{up}}\right), \ldots, \left(m - \left|\frac{ppr}{2}\right|_{\mathrm{down}}\right)$, with $\left|\frac{ppr}{2}\right|_{\mathrm{up}}$ and $\left|\frac{ppr}{2}\right|_{\mathrm{down}}$ equal to half of ppr rounded up and down, respectively.

The shaft rotational speed, $n\,(t_j)$, is then calculated as the average of those two speeds to minimise the error:

$$n\,(t_j) = \frac{n_1\,(t_{1,j}) + n_2\,(t_{2,j})}{2} \tag{10}$$

where t_j is given by:

$$t_j = \frac{t_{1,j} + t_{2,j}}{2}. \tag{11}$$

3.3.3. Shaft absolute twist.

3.3.3.1.Time shift measurement by direct timing of rising edges. The rising edge detection approach is the most straightforward method for determining the time delay between the pulses. It is based on the measurement of the times at which the rising edges of the two pulse trains occur and on the calculation of their relative phase shift, as shown in figure 10. In the rising edge detection approach VI, the time shift between the two pulse trains associated with the signals' average rising edge times, $\Delta t_r\,(\overline{t_{i\mathrm{OP}'}})$, is calculated as:

$$\Delta t_r\,(\overline{t_{i\mathrm{OP}'}}) = t_{i\mathrm{OP}'_2} - t_{i\mathrm{OP}'_1} \tag{12}$$

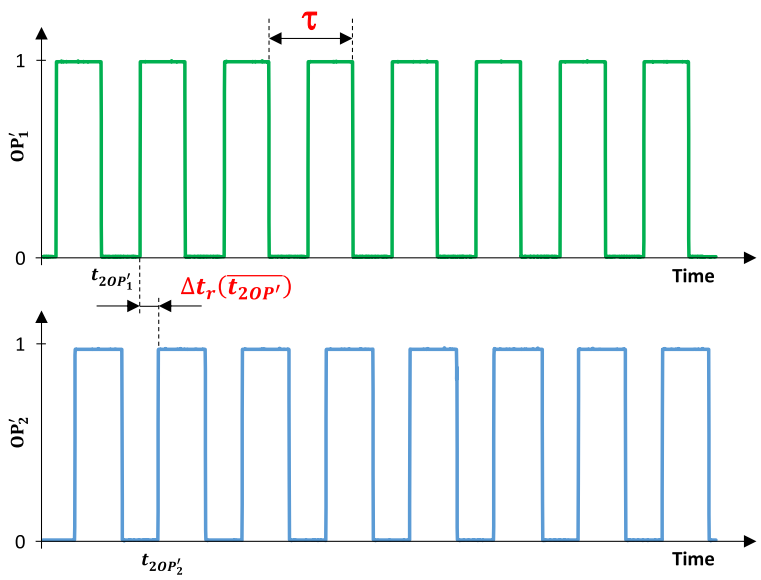

Figure 10. Phase shift estimation through the rising edge detection approach.

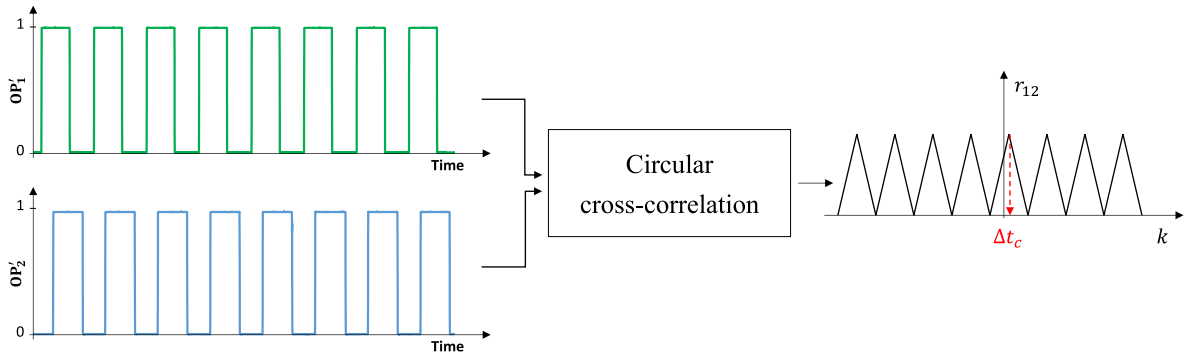

Figure 11. Phase shift estimation through the cross-correlation approach.

where $i = 1,\ldots..,\ m$ and $\overline{t_{i\mathrm{OP}'}}$ is defined as:

$$\overline{t_{i\mathrm{OP}'}} = \frac{t_{i\mathrm{OP}'_1} + t_{i\mathrm{OP}'_2}}{2}. \tag{13}$$

As already pointed out, tangential and radial displacements between shaft and OPs, typically caused by vibrations or shaft deformation, introduce noise in timing of pulses. This noise is expected to be periodic, at the rotational frequency or its harmonics. Therefore, a moving average filter is implemented to measure a time delay averaged over a full revolution $\overline{\Delta t}_{\mathrm{r}}(t_j)$. This is implemented as moving average filter over the eight delays $\Delta t_{\mathrm{r}}(\overline{t_{i\mathrm{OP}'}})$ measured during a full revolution, with seven-point overlap over time, allowing the calculation of an averaged delay for each pulse, that is one value per zebra tape pulse.

The eight-point averaged time shift, $\overline{\Delta t}_{\mathrm{r}}(t_j)$, is calculated as:

$$\overline{\Delta t}_{\mathrm{r}}(t_j) = \sum_{i=j+1-\left|\frac{ppr}{2}\right|_{\mathrm{up}}}^{j+\left|\frac{ppr}{2}\right|_{\mathrm{down}}} \frac{\Delta t_{\mathrm{r}}(\overline{t_{i\mathrm{OP}'}})}{ppr}. \tag{14}$$

3.3.3.2.Time shift measurement by cross-correlation. The cross-correlation approach allows the measurement of the similarity of the two time series, OP'_1 and OP'_2, as a function of the time-lag applied to one of them. Unlike the rising edge detection approach, the cross-correlation VI uses the full initialised signals OP'_1 and OP'_2 to estimate their time shift and not only the times at which the rising edges occur (figure 11).

Cross-correlation is implemented according to [28], as circular cross-correlation, defined as:

$$r_{12}(k) = \frac{1}{N}\sum_{n=0}^{N-1} \mathrm{OP}'_1(n)\,\mathrm{OP}'_2(k-n) \tag{15}$$

where $k = 0,\ldots,\ N-1$ and N, the length of the two signals, is chosen equal to the shaft revolution. This algorithm does not require zero padding, but considers the pulse train to be periodic.

Circular cross-correlation provides an output with 8 peaks, equal to the number of pulses per revolution (figure 11), that correspond to 8 possible time delays, as usual in a periodic function. The delay of interest is the smallest one, Δt_{c}, provided that the zebra tape period is larger than the maximum shift, as discussed in section 3.1, equation (5). The other peaks appear because the train of pulses is a periodic function.

The signals OP'_1 and OP'_2 are progressively circular cross-correlated giving one value of the time shift per zebra tape

pulse, $\Delta t_c\,(t_j)$, similarly to the case of the rising edge detection approach $\overline{\Delta t}_r\,(t_j)$.

In both approaches, the calculated time shifts, $\overline{\Delta t}_r\,(t_j)$ and $\Delta t_c\,(t_j)$, respectively, depend on the shaft speed. According to equation (4), they are converted into shaft absolute angular shifts, $\theta_{a\_r}\,(t_j)$ and $\theta_{a\_c}\,(t_j)$, respectively, by:

$$\theta_{a\_r}\,(t_j) = \frac{2\pi}{60} n\,(t_j)\,\overline{\Delta t}_r\,(t_j) \tag{16}$$

$$\theta_{a\_c}\,(t_j) = \frac{2\pi}{60} n\,(t_j)\,\Delta t_c\,(t_j)\,. \tag{17}$$

3.4. Range, resolution and sampling frequency

For a given zebra tape design (ppr), shaft speed (n) and OP sampling frequency (f_{OP}), the non-intrusive torque measurement system features are:

$$\text{Range:} \qquad \theta_{RANGE} = [-\theta_{full_{scale}}, \theta_{full\_scale}] = \left[-\frac{\pi}{ppr}, \frac{\pi}{ppr}\right] \tag{18}$$

$$\text{Resolution:} \qquad \delta\theta = \frac{2\pi n}{60} * \frac{1}{f_{OP}}. \tag{19}$$

Using the calibration curve, $\theta = m * T$, where m is the calibration line slope, equations (18) and (19) allow the estimation of the corresponding torque range T_{RANGE} and resolution δT.

$$T_{RANGE} = \frac{\theta_{RANGE}}{m} \tag{20}$$

$$\delta T = \frac{\delta\theta}{m} \tag{21}$$

$$\text{Sampling Frequency:} \qquad f_c = \frac{2\pi n}{60} * \frac{ppr}{2\pi} = \frac{n * ppr}{60}. \tag{22}$$

Torque samples are then obtained at a non-constant frequency which is dependent on the shaft speed.

4. Calibration and uncertainty analysis

4.1. System calibration

The non-contact optical torque system was calibrated against reference torque measurements from the in-line torque transducer in order to fully characterise the torque-twist angle relationship described by equation (1). The calibration curve allows the estimation of the torque acting along the shaft by simply recording the zebra tape pulse trains, calculating their time shift and hence the shaft angular shift, using either method.

Steady state tests were performed on the test rig at four different shaft speeds: 1600, 1700, 1800 and 1900 rpm. For each speed, the calibration procedure consisted of the following steps:

(1) Run the motor to the required testing speed.
(2) Record the signals from both the OPs and the torque transducer at no-load (0 V applied to the generator stator) for around 10 s.
(3) Vary the generator stator voltage to increase the shaft torque in steps of 2 N m, starting from an initial torque value of 1 N m in the case of the tests run at 1600 and 1800 rpm and 2 N m in the case of the tests run at 1700 and 1900 rpm. For each speed, to avoid damage to the generator during operation, the stator voltage was varied up to a precautionary safety limit of its armature winding current of 8 Amps; this determined the maximum operational torque. Given the available experimental set-up, the calibration range was limited to 16 N m, even though the zebra tape had been designed with a period allowing measurements up to 62 N m, which therefore represents its full-scale input range.
(4) Record the signals from both the OPs and the torque transducer for around 10 s for each applied torque level.
(5) Post-process the OP pulse data and calculate the shaft twist using the rising edge detection and cross-correlation approaches presented in section 3.3.
(6) Build calibration curves by plotting the shaft relative twist, calculated according to equation (4), against the corresponding reference torque measured by the in-line transducer, whose signal was resampled to match the time delay sampling frequency.

The calibration curves resulting from the rising edge and the cross-correlation approaches are shown in figures 12 and 13, respectively, and compared in table 2. They result from the linear regression of experimental data by a straight line using the least square method. As predicted by equation (1), the torque-twist trend is linear under steady state conditions. The two calibration curves show a similar trend with satisfactory R-squared levels, indicating a good fit of the experimental data by the regression line. A difference in sensitivity of around 2% is observed.

4.2. Measurement uncertainty evaluation

The measurement uncertainty has been estimated according to the ISO GUM (Guide to the expression of uncertainty in measurement). The statistical processing of series of experimental data obtained in the laboratory conditions has allowed a Type A uncertainty estimation. A more comprehensive Type B analysis has been performed using the Monte Carlo method, where a number of influencing parameters and disturbances which could affect the measurement system in a real-world application has been considered.

4.2.1. Type A uncertainty. The regression of calibration data has allowed the statistical estimation of the Type A uncertainty of measurement, U_{exp} (table 2), with respect to the maximum torque achievable during operation (16 N m), which corresponds to 26% of the torque meter full operating range.

For each case, the standard deviation of the input torque, s_T, has been estimated by statistical analysis of the residuals of the M calibration data with respect to their interpolating line as:

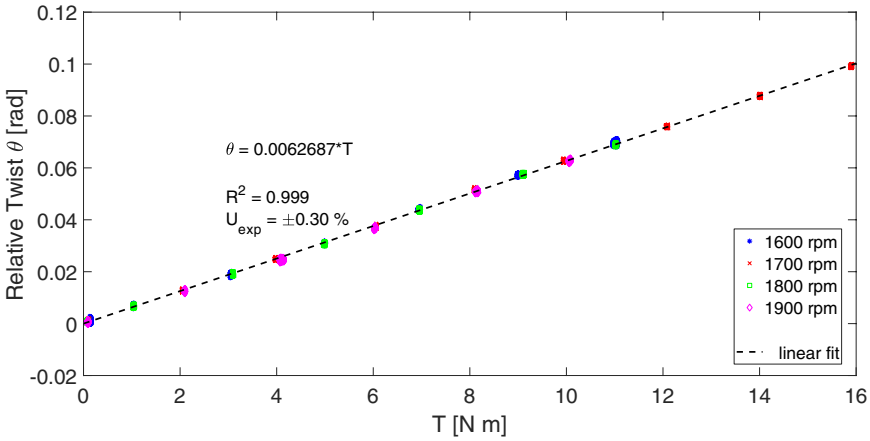

Figure 12. Calibration curve: Rising edge detection approach.

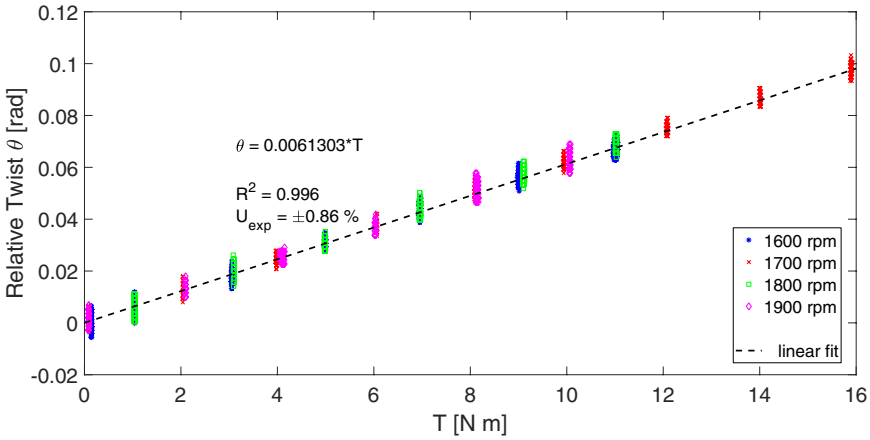

Figure 13. Calibration curve: cross-correlation approach.

Table 2. Parameters of the two calibration curves and their Type A expanded uncertainty relative to the system full-scale torque, U_{exp}.

Method	Linear fit equation	R^2	U_{exp} (%)
Rising edge	$\theta = 6.2687\ 10^{-3} * \mathrm{T}$	0.999	±0.30
Cross-correlation	$\theta = 6.1303\ 10^{-3} * \mathrm{T}$	0.996	±0.86

$$s_{\mathrm{T}} = \sqrt{\frac{1}{M-2}\sum_{k=1}^{M}\left(\frac{\theta_k}{m} - T_k\right)^2} \tag{23}$$

where θ is the shaft relative twist predicted by the calibration line. The type A uncertainty relative to the system full-scale torque, U_{exp}, associated with each approach has then been calculated, in compliance with the ISO GUM:1995 [29], as expanded uncertainty with a coverage factor $k = 2$, allowing for a 95% confidence level, as:

$$U_{exp}(\mathrm{N\,m}) = k s_{\mathrm{T}} \tag{24}$$

and expressed as a percentage of the measurement system full-scale torque, T_{full_scale}, as:

$$U_{exp}(\%) = \frac{u_{exp}(\mathrm{N\,m})}{T_{full\_scale}(\mathrm{N\,m})} 100 \tag{25}$$

where:

$$T_{full\_scale} = \frac{\theta_{full\_scale}}{m} \tag{26}$$

and θ_{full_scale} is the measurement system full-scale twist output given in table 1.

In this analysis, the same statistical uncertainty has been assumed all over the entire operating range, even if this has been estimated by using available experimental data referring to the first 26% of the torque meter design range.

The type A uncertainty analysis has taken into account experiments at various speed and torque levels, which were repeated over several days and performed by different operators. This provides information on repeatability and reproducibility of the proposed method.

For the experimental set-up used in this work, the maximum measurable angular shift of the system corresponds to the full-scale input torque $T_{RANGE} = 62\,\mathrm{N\,m}$, which is approximately four times larger than the calibration range. Within this range the system has a resolution δT of 0.27 N m if only one rising edge is used; however, the resolution decreases by *ppr* if the angular shift is determined by averaging a series of *ppr* angular shifts. In this case $ppr = 8$ was used.

Unexpectedly, the cross-correlation approach results show a higher dispersion around their best fit curve when compared to the rising edge detection approach, resulting in higher uncertainty of the method (table 2). Cross-correlation underperforms

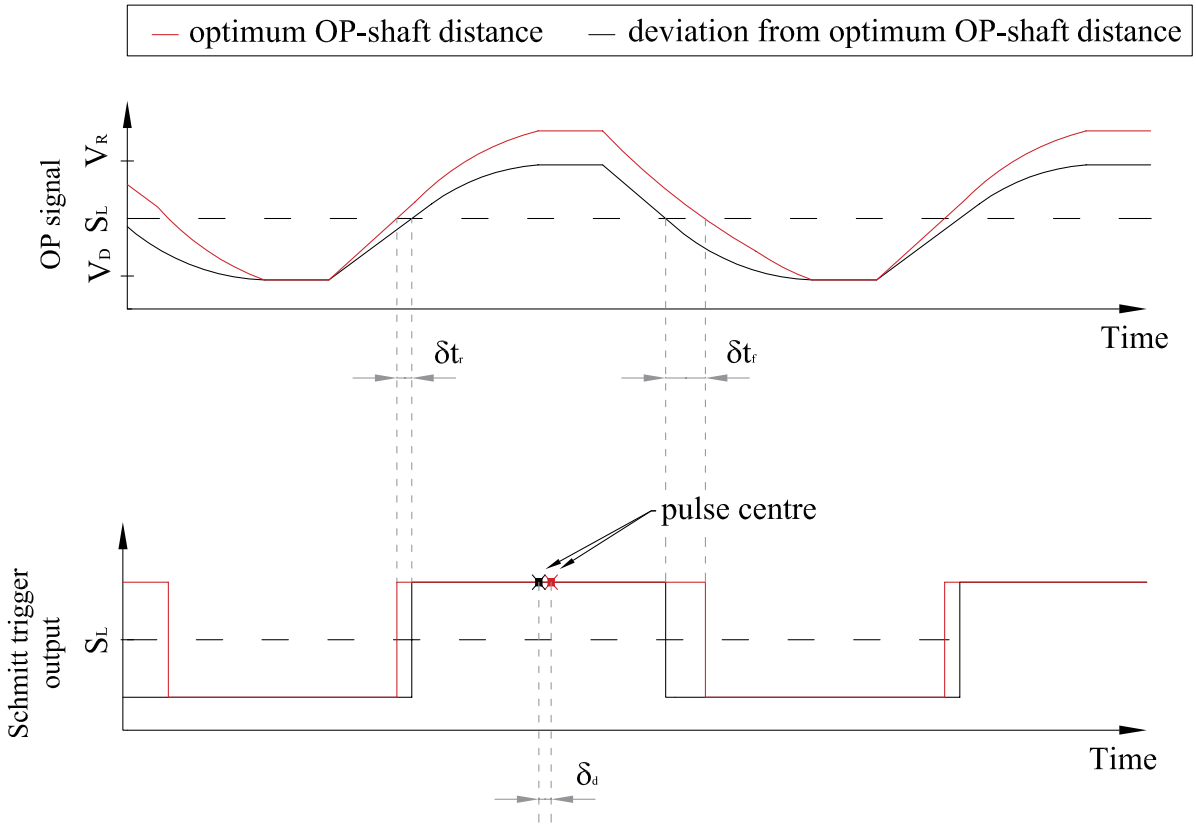

Figure 14. Effect of sensor to shaft distance variation on the OP output.

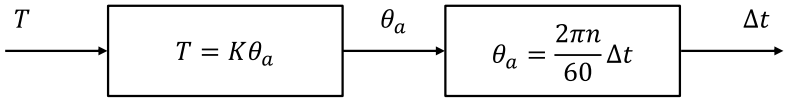

Figure 15. Zebra tape torque meter model.

with respect to direct timing because of the changes in duty cycle throughout one shaft revolution and the time shift introduced by the Schmidt trigger operating on an amplitude modulated photodetector signal. As mentioned, amplitude modulation may affect the optical signal because of possible vibrations, shaft misalignment or bending; all these phenomena would affect the sensor to shaft distance during shaft rotation. In these conditions, after the Schmidt trigger, the variation of duty cycle and time shift causes a displacement of the pulse centre equal to $\delta_d = (\delta t_r + \delta t_f)/2$, as shown in figure 14.

Cross-correlation is more sensitive to pulse shape than rising edge timing. Moreover, cross-correlation is intrinsically sensitive to the position of the centre of each square pulse. These effects together explain the larger dispersion of data seen for cross-correlation whenever the optical signal experiences amplitude modulation and a Schmidt trigger is applied. It would therefore be expected that cross-correlation would better perform on the original photodetector signal, before being squared by the Schmidt, but this has not been implemented in this paper.

4.2.2. Uncertainty analysis using Monte Carlo method (MCM). The propagation of distributions through a mathematical model of the zebra tape torque meter system has been implemented by MCM for the evaluation of uncertainty of measurement according to the GUM:1995 Supplement 1 [30].

Table 3. Measurement system model equations.

Method	Model
Rising edge detection	$T = K\frac{2\pi n}{60}\overline{\Delta t_r}$
Cross-correlation	$T = K\frac{2\pi n}{60}\Delta t_c$

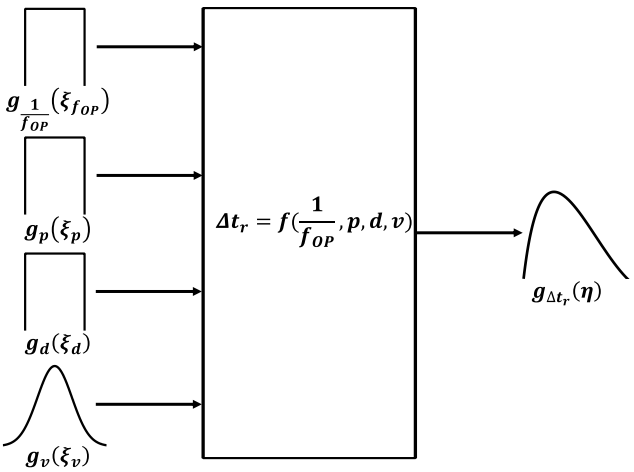

Figure 16. PDF propagation of the four independent input quantities to provide the PDF of Δt_r (Adapted with permission from [30]. Permission to reproduce extracts from ISO publications is granted by BSI Standards Limited (BSI) on behalf of International Organization for Standardization (ISO). No other use of this material is permitted.)

Table 4. Uncertainties and sensitivity analysis of the quantities contributing to $u_{\Delta t_r}$.

X_j				
Symbol	Name	Standard deviation s_j	Half-width tolerance a_j	Sensitivity analysis $\left(\frac{\widehat{df}}{dx_j}\right)^2 ux_i^2$
$\frac{1}{f_{OP}}$	OP sampling frequency		$4.00 * 10^{-6}$ (s)	$1.33 * 10^{-12}$ (s)
p	Zebra tape laser-printing		$2.12 * 10^{-5}$ (m)[a]	$2.76 * 10^{-7}$ (s)
d	Shaft cylindricity error		$33 * 10^{-6}$ (m)[a]	$4.30 * 10^{-7}$ (s)
v	Shaft movements	$60 * 10^{-6}$ (m)[a]		$5.63 * 10^{-10}$ (s)

[a] Model assumption.

The measurement uncertainty evaluation has been performed with respect to a shaft rotational speed of 1700 rpm at which the maximum torque achievable during operation (16 N m) was measured.

A mathematical model of the zebra tape torque meter, shown schematically in figure 15, has been built to relate the output quantity T (i.e. the quantity intended to be measured) with the input quantities $\boldsymbol{X}$ (i.e. K, n and Δt) upon which T depends. Table 3 summarises the model equations for the two approaches.

The shaft torsional stiffness, K, has been estimated as the inverse of the slope of the rising edge calibration linear fit equation and its standard deviation, s_K, has been computed by Type A method according to the GUM [29], that is by performing a statistical analysis of the residuals of the M calibration data with respect to its inverse interpolating line $T = K\theta$ as:

$$s_K = \sqrt{\frac{M s_T^2}{M\sum_{j=1}^{M}\theta_j^2 - \left(\sum_{j=1}^{M}\theta_j\right)^2}}. \tag{27}$$

The uncertainty of the shaft angular speed n is computed by Type A method, by performing a statistical analysis of the time series of experimental data from the torque test rig at steady state, according to the GUM [29]. The standard uncertainty s_n is therefore computed as standard deviation of n, and results to be:

$$s_n = 0.23\ (\text{rpm}). \tag{28}$$

In the case of the rising edge approach, the probability density function (PDF) for the time shift measured by direct timing of each pair of rising edges, $g_{\Delta t_r}(\eta)$, has been computed through MCM, where 10^6 simulations have been performed to deliver a 95% coverage interval for the output quantity according to [30]. In this case $g_{\Delta t_r}(\eta)$ depends on the propagation through the model of the PDFs of the following independent input quantities (figure 16), each with its own statistical dispersion:

- the time interval between the OP samples, with an associated rectangular PDF and $2a_{\frac{1}{f_{OP}}}$ width, where:

$$a_{\frac{1}{f_{OP}}} = \frac{1}{2 * f_{OP}} \tag{29}$$

- the zebra tape laser-printing resolution, with an associated rectangular PDF and $2a_p$ width, where, assuming a 1200 dpi laser printer, the printing tolerance, a_p, is given by:

$$a_p = \frac{\left(25.4 * 10^{-3}\right)}{1200} = 2.128 * 10^{-5}\ (\text{m}) \tag{30}$$

- the shaft cylindricity error, with an associated rectangular PDF and $2a_d$ width, where, assuming an IT8 tolerance class of the shaft, its dimensional tolerance, a_d is given by [31];
- the shaft radial movements (possibly due to vibrations), assumed to act in the direction perpendicular to the optical sensor axis, with associated Gaussian PDF and an assumed standard deviation of:

$$s_v = 60 * 10^{-6}\ (\text{m}). \tag{31}$$

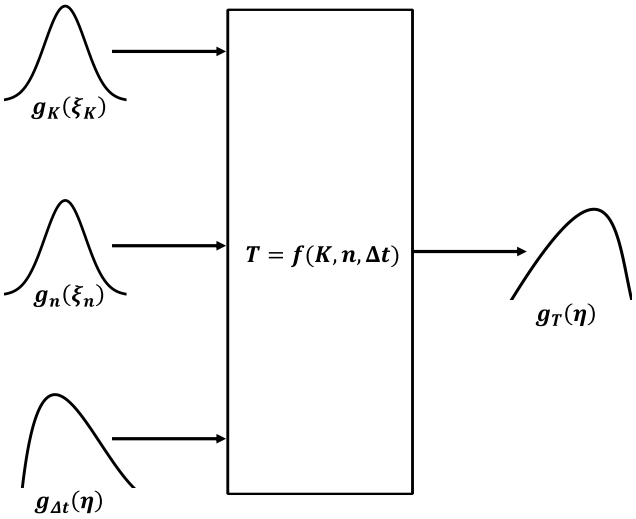

Figure 17. PDF propagation of K, n and Δt to provide the PDF of T through the zebra tape torque meter model (Adapted with permission from [30]. Permission to reproduce extracts from ISO publications is granted by BSI Standards Limited (BSI) on behalf of International Organization for Standardization (ISO). No other use of this material is permitted.)

Table 4 summarises the input parameters contributing to the uncertainty of Δt_r, $u_{\Delta t_r}$, each with its associated uncertainty intervals used in the model. The amplitude of these intervals has been assumed based on knowledge of the technology implemented in the system; it is either the width of a flat PDF or the standard deviation of a Gaussian PDF, depending on the type of parameter. The table also provides a sensitivity

Table 5. Uncertainties and sensitivity analysis of the quantities contributing to u_T.

X_j			Standard deviation s_j	Sensitivity analysis	
Symbol	Name	Value		Rising edge	Cross-correlation
K	Shaft torsional stiffness	159.523 N m rad^{-1}[a]	0.0077 N m rad^{-1}[a]	$5.965 * 10^{-7}$ (N m)	$5.965 * 10^{-7}$ (N m)
n	Shaft rotational speed	1700 (rpm)[a]	0.23 (rpm)[a]	$4.686 * 10^{-6}$ (N m)	$4.686 * 10^{-6}$ (N m)
$\overline{\Delta t_r}$	Time shift measurement by direct timing of rising edges	$5.634 * 10^{-4}$ (s)[a]	$1.272 * 10^{-5}$ (s)[b]	0.131 (N m)	
$\overline{\Delta t_c}$	Time shift measurement by cross-correlation	$5.509 * 10^{-4}$ (s)[a]	$1.273 * 10^{-5}$ (s)[b]		0.137 (N m)

[a] Experimental result.
[b] MCM result.

Table 6. Torque meter system Type B expanded uncertainty relative to the system full-scale torque, U_{MCM}.

Method	U_{MCM} (%)
Rising edge	±1.17
Cross-correlation	±1.19

analysis, that is an estimate of the contribution to the overall uncertainty budget for each input parameter, showing that the zebra tape laser-printing and the shaft cylindricity errors are the major contributors to $u_{\Delta t_r}$.

Within each shaft revolution, the standard deviation of $\overline{\Delta t_r}$, $s_{\overline{\Delta t_r}}$, has then been then obtained through MCM as the average of the eight pulse train rising edges, Δt_r, and their PDFs, $g_{\Delta t_r}$.

In the case of the cross-correlation approach, the same Gaussian PDF, with uncertainty $u_{\Delta t_r}$, has been assumed for all the time shifts measured between the rising and falling edges, respectively. Unlike the rising edge detection approach, in this case the standard deviation of Δt_c, $s_{u_{\Delta t_c}}$, has been obtained by type B analysis [29] as:

$$s_{\Delta t_c} = \frac{u_{\Delta t_r}}{\sqrt{2ppr}}. \tag{32}$$

The PDF for T, $g_T(\eta)$, depends on the propagation through the model of the PDFs of the independent input quantities, K, n and Δt ($\overline{\Delta t_r}$ or Δt_c, depending on the approach adopted) as described in figure 17.

Table 5 summarises the quantities used for the estimation of the uncertainty of T, u_T, and their sensitivity analysis, showing that, in both approaches, the estimation of Δt is the major contributor to u_T.

For both approaches, table 6 shows the torque measurement type B expanded uncertainty at 95% confidence level (i.e. corresponding to two standard deviations) obtained by applying the MCM in compliance with the ISO GUM [30] and expressed as a percentage of the system full-scale torque T_{full_scale}.

In both cases, the results show that the application of the MCM to a simplified model of the measurement system overestimates the overall uncertainty when compared to the type A uncertainty obtained by experimental results, as reported in table 2. The rising edge detection approach shows the larger difference between the values of U_{MCM} and U_{exp}. Indeed, it is reasonable that a type A evaluation based on laboratory data underestimates uncertainty, given that MCM takes into account all possible sources of uncertainty which may occur in real-world applications and not in the controlled laboratory environment. This explains the lower value of uncertainty obtained through statistical processing of the experimental data. Therefore, the uncertainty estimated by MCM sets the maximum value of the system uncertainty attainable in practical applications.

5. Results

Tests have been performed to validate the proposed zebra-tape torque meter under both static and variable conditions. The torque measurements obtained by the zebra tape torque meter have been compared with measurements from the in-line torque transducer (Magtrol) which has been assumed as the reference system for all the experimental work, being a well-established state-of-the-art technique. Shaft speed was also recorded by the zebra tapes.

5.1. Steady state tests

Figure 18 shows speed and torque results for two steady state tests performed at 1700 rpm, 4 N m and 1900 rpm, 10 N m.

Both the cross-correlation (azure solid line) and rising edge (red solid line) approaches show good agreement, on average, with reference transducer measurements (black dotted line) however the zebra tape data appears noisier. This is particularly apparent for torque measurements obtained by cross-correlation. The causes of noise in this data have been already outlined when showing the calibration results however it should also be noted that the reference transducer is sampled at a much lower rate, possibly reducing its own noise levels. The frequency at which noise appears for the optical system is significantly higher than any relevant frequencies expected in the mechanical torque signal therefore such noise could be reduced by low pass digital filtering.

5.2. Variable torque and speed tests

Finally, variable torque and speed tests have been performed to evaluate and compare the response of the two approaches. Figure 19 shows the effects of sharp step changes in torque.

The shaft speed was initially set at around 1715 rpm and the torque first increased and then decreased in steps of approximately 2 N m, in the 0–15 N m operating range. Changes in

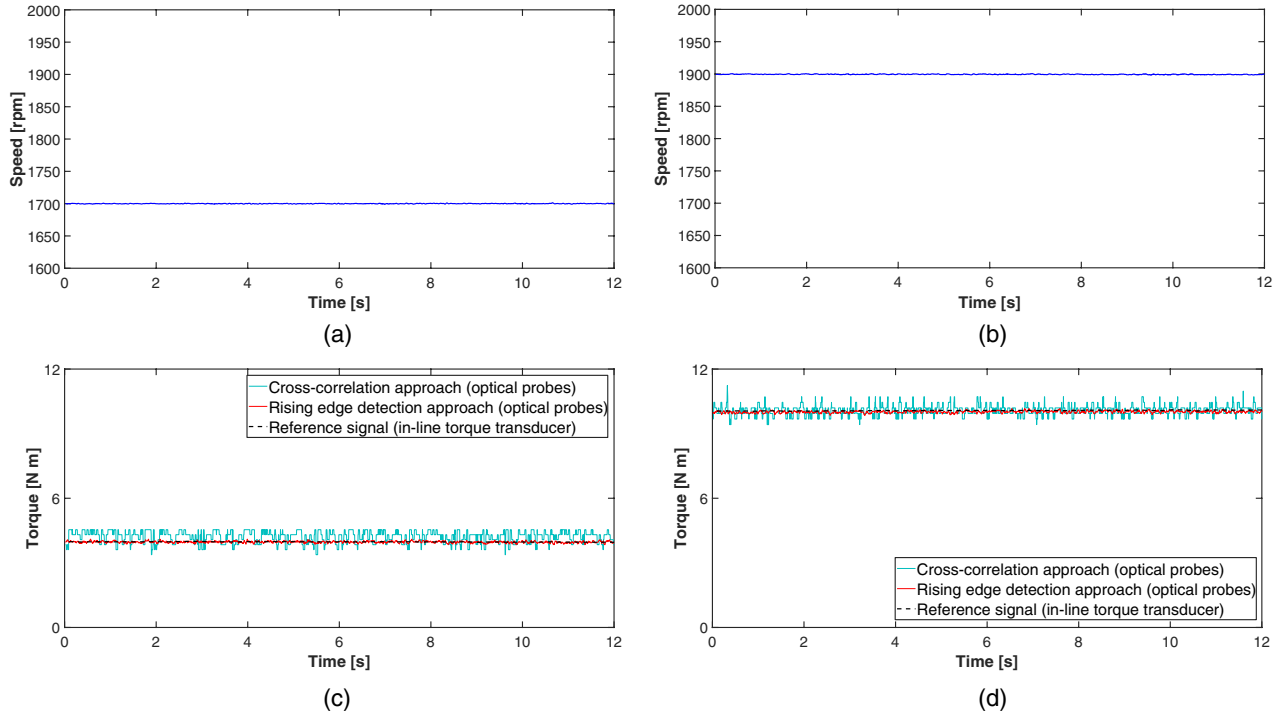

Figure 18. Optical system speed and torque measurement under steady state conditions: (a) and (c) 1700 rpm and 4 N m; (b) and (d) 1900 rpm and 10 N m.

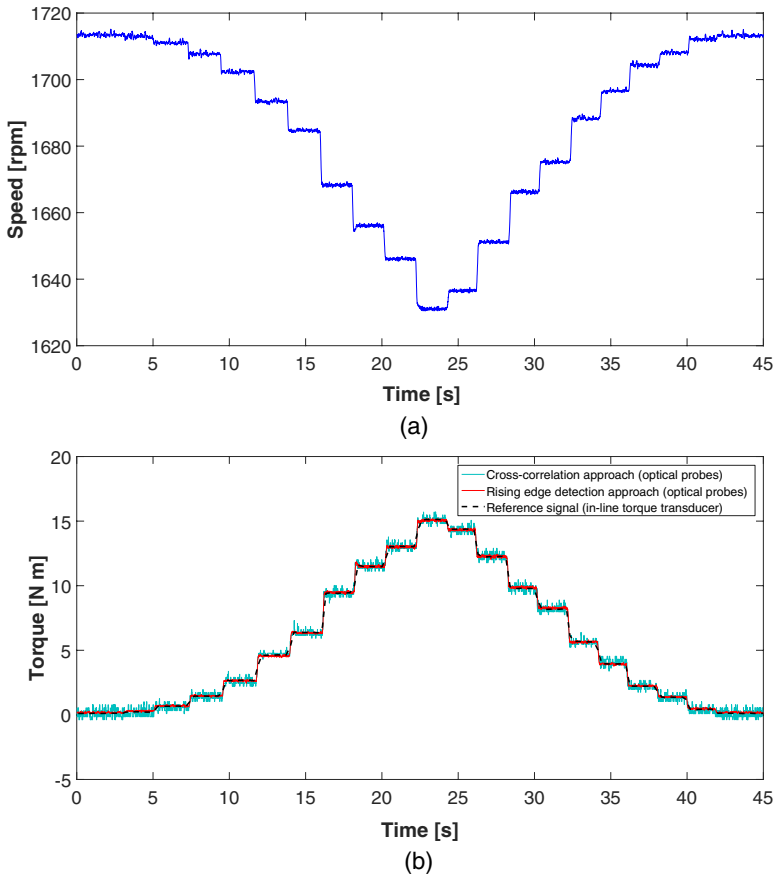

Figure 19. Optical system speed (a) and torque (b) measurements under sharp step torque changes.

speed are the result of applied torque that were not countered by the variable speed drive. The zebra tape measurements allow tracking of the rotational frequency as well as the torque during the whole transient. The response of the zebra tape torque meter under variable torque and speed test conditions is sufficient to track the torque variations imposed on the shaft.

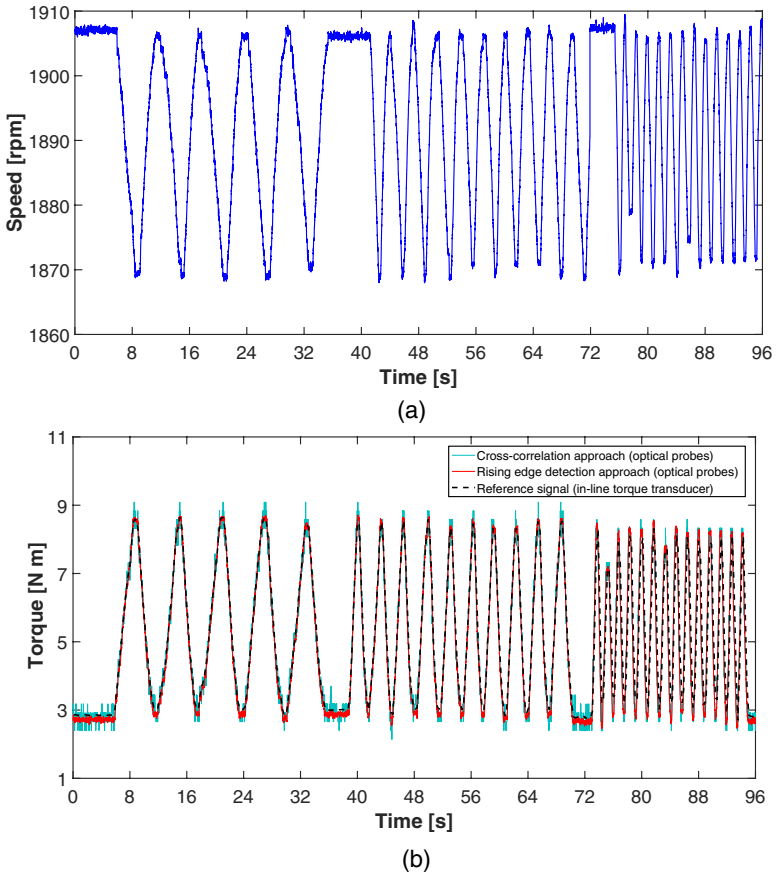

Figure 20. Optical system speed (a) and torque (b) measurements under torque varying at three different frequencies (0.17 Hz, 0.30 Hz and 0.63 Hz).

Both the rising edge and cross correlation torque estimations follow the step changes well and without any timing delay. However, as already noted, the outputs are noisier, especially when the cross-correlation approach is applied. Low pass filtering would reduce this noise without affecting torque meter response in the band of frequencies of interest for mechanical torque measurements.

Additional variable torque and speed tests have been performed by applying a harmonic input torque at three different frequencies (0.17 Hz, 0.30 Hz and 0.63 Hz) and at a peak-to-peak amplitude of approximately 6 N m (figures 20(a) and (b)), within experimental limitations. Again, the zebra tape torque meter shows a good response under harmonic changes of input torque, even if affected by greater high frequency noise in the case of the cross-correlation approach.

6. Comparison with conventional twist angle measurement methods

Similarly to the conventional twist angle measurement methods [7, 13–15], the time shift between the signals recorded by the two zebra tape torque meter OPs is a function of the twist of the shaft due to the applied torque. However, the non-intrusive system presented in this paper has the significant advantages of using less-intrusive, cheaper, easier and quicker to install equipment, making it suitable for a larger range of industrial applications, even in confined, challenging or sensitive operating environments, without any significant impact on shaft design and mechanical integrity. In addition to torque measurement, the zebra tape torque meter provides the shaft rotational speed, which allows the measurement of the mechanical power transmitted by the shaft. This results in a reduction in the number of sensors in the system and hence saving in space, weight and complexity, which is particularly important for many industrial applications, such as in the naval and wind energy sectors. The measurement system is reliable, robust and straightforward to use. The zebra tapes can be designed to be fitted or retrofitted on any shaft diameter and material, while all the electronic components remain on the static part of the system, making the system compatible with harsh and polluted environments. High measurement accuracy and resolution can be achieved by accurately designing the width of the zebra tape black and white stripes to suit the particular application. Thanks to the easy glue-on installation of the zebra tapes, the measurement system can be moved to other similar installations easily in a very short amount of time. This is ideal when torque monitoring forms part of the final check-out of multiple machines. By simply modifying the separation distance of the two zebra tapes along the shaft, when its length allows, different measurement sensitivities can be achieved according to the field application requirements. This would generally result in

sensitivities higher than conventional optical torque measurement systems.

7. Conclusions

This paper presents a non-intrusive technique for shaft speed and torque measurement consisting of a set of two zebra tapes and OPs, one at each end of the shaft. The method has been experimentally implemented and validated under both static and variable conditions. The following specific conclusions arise:

- As the shaft rotates, each optical sensor generates a pulse train signal proportional to the light intensity reflected by the zebra tape stripes. Shaft rotational speed has been calculated by measuring the times at which the rising edges of the pulse trains occur.
- Torque has been estimated by measuring the angle of twist from the pulse train time shift measurements through the application of rising edge detection and cross-correlation approaches.
- The contactless, optical torque measurement system performance has been demonstrated by comparing the results from both approaches against reference measurements from an in-line torque transducer mounted on the test bench shaft.
- Experimental measurements under steady state conditions, performed to calibrate the contactless system, show a linear relationship between torque and twist, in perfect agreement with theoretical predictions.
- Uncertainty has been estimated according to the ISO GUM. Type A analysis of experimental data has provided an expanded uncertainty relative to the system full-scale torque, of $\pm 0.30\%$ for the rising edge approach and $\pm 0.86\%$ for the cross-correlation approach. Statistical variations of the parameters affecting system performance under real-world operating conditions have been simulated through the Monte Carlo method providing, in the worst case, an estimation of the system expanded uncertainty of $\pm 1.19\%$.
- The higher uncertainty associated with the cross-correlation method is shown to be due to the combined effect of its higher sensitivity to the pulse shape and to the position of its centre. Low pass digital filtering would reduce the noise associated with the cross-correlation approach without affecting the torque meter response.
- The rising edge and the cross-correlation torque measurements correlate closely with the in-line transducer measurements under both steady state and variable test conditions, although showing a higher level of noise.
- Unlike conventional in-line torque transducers and the conventional strain gauge technique, the proposed zebra tape torque meter does not require costly embedded sensors, electronics or wires on the rotating shaft. Comparing with conventional twist angle measurement methods, the proposed methodology is less intrusive, simpler and cheaper to implement, making it suitable to a larger variety of engineering applications. Measurement accuracy and resolution can be easily adapted to the field application requirements by carefully designing the zebra tapes and their separation along the shaft.

Acknowledgments

This work was funded as part of the UK EPSRC SUPERGEN Wind Hub, EP/L014106/1. The data presented in this paper are available from the Durham Research Online Data Depository at https://doi.org/10.15128/r1v979v306n.

ORCID iDs

D Zappalá https://orcid.org/0000-0002-8283-5102
C J Crabtree https://orcid.org/0000-0003-0109-5323
N Paone https://orcid.org/0000-0002-1228-8967

References

[1] van Millingen R D and van Millingen J D 1991 Phase shift torquemeters for gas turbine development and monitoring *Proc. ASME Int. Gas Turbine and Aeroengine Congress and Exposition (Orlando, FL, 3–6 June)* vol 5 (https://doi.org/10.1115/91-GT-189)
[2] Petek J and Hamilton P 2005 Performance monitoring for gas turbines *Orbit* **25** 65–74
[3] Vath A and Grimm S 2015 Reliability and energy yield increase of wind turbines as a benefit of dynamic load reduction operation *Proc. Scientific Track of the European Wind Energy Association Conf. (Paris, France, 17–20 November 2015)*
[4] Hackl C M and Schechner K 2016 Non-ideal feedforward torque control of wind turbines: impacts on annual energy production & gross earnings *J. Phys.: Conf. Ser.* **753** 1–10
[5] Soong W and Ertugrul N 2002 Field-weakening performance of interior permanent-magnet motors *IEEE Trans. Ind. Appl.* **38** 1251–8
[6] Boyer F, Porez M and Khalil W 2006 Macro-continuous computed torque algorithm for a three-dimensional eel-like robot *IEEE Trans. Robot.* **22** 763–75
[7] Austin C and Rojon I 2014 *Ship Performance Management* (Windsor: Fathom)
[8] Fleming W J 1982 Automotive torque measurement: a summary of seven different methods *IEEE Trans. Veh. Technol.* **3** 117–24
[9] Guy B 2015 Measurement and traceability of torque on large mechanical drives *Proc. AMA Conf.—SENSOR 2015 and IRS2 2015 (Nuremberg, Germany, 19–21 May 2015)* pp 44–5
[10] Cichowicz J, Gerasimos T and Dracos V 2015 Dynamic energy modelling for ship life-cycle performance assessment *Ocean Eng.* **110** 49–61
[11] Nazar Ul Islam M, Cheng P and Oelmann B 2016 Method of torque measurement based on volumetric strain *Proc. SICE Annual Conf. (Tsukuba, Japan, 20–23 September 2016)* pp 116–23
[12] Lee K-E, Kim J-W, Kim C-Y and Ahn S-H 2009 Development of micro torque measurement device using strain gauge *Proc. IEEE Int. Symp. on Assembly and Manufacturing, ISAM 2009 (Suwon, Korea, 17–20 November 2009)* pp 101–6

[13] de Silva C W 2015 *Sensors and Actuators: Engineering System Instrumentation* 2nd edn (Boca Raton, FL: CRC Press)
[14] Shams S, Lee J Y and Han C 2012 Compact and lightweight optical torque sensor for robots with increased range *Sensors Actuators* A **173** 81–9
[15] Hazelden R J 1993 Optical torque sensor for automotive steering systems *Sensors Actuators* A **37–8** 193–7
[16] Wilmshurst T H, Rothberg S J and Halliwell N A 1991 Laser torquemeter: a new instrument *Electron. Lett.* **27** 186–7
[17] Tullis I D C, Halliwell N A and Rothberg S J 1996 Laser torquemeter: effects of axial shaft vibration *Proc. SPIE* **2868** 449–57
[18] Tullis I D C, Halliwell N A and Rothberg S J 1998 Shaft tilt sensitivity of the laser torquemeter *Proc. SPIE* **3411** 309–16
[19] Garinei A and Marsili R 2017 Development of a non-contact torque transducer based on the laser speckle contrast method *J. Sensors Sensor Syst.* **6** 253–8
[20] Hajdu F and Horváth P 2012 Contactless torque sensor development *Acta Tech. J.* **5** 115–20
[21] Angleviel D, Frachon D and Masson G 2006 Development of a contactless hall effect torque sensor for electric power steering *Proc. SAE 2006 Automotive Dynamics Stability and Controls Conf. and Exhibition (Novi, Michigan, 14–16 February 2006)* (https://doi.org/10.4271/2006-01-0939)
[22] Seidlitz S, Kuether R J and Allen M S 2016 Experimental approach to compare noise floors of various torsional vibration sensors *Exp. Tech.* **40** 661–75
[23] Janssens K, Van Vlierberghe P, D'Hondt P, Martens T, Peeters B and Claes W 2011 Zebra tape butt joint algorithm for torsional vibrations *Structural Dynamics* (*Conf. Proc. of the Society for Experimental Mechanics Series* vol 3) ed T Proulx (New York: Springer) (https://doi.org/10.1007/978-1-4419-9834-7_19)
[24] Friswel M I, Penny J E T, Garvey S D and Lees A W 2010 *Dynamics of Rotating Machines* (Cambridge: Cambridge University Press) (https://doi.org/10.1017/CBO9780511780509)
[25] Sue P, Wilson D, Farr L and Kretschmar A 2012 High precision torque measurement on a rotating load coupling for power generation operations *Proc. IEEE Int. Instrumentation and Measurement Technology Conf. (I2MTC) (Graz, Austria, 13–16 May 2012)* pp 518–23
[26] Janssens K and Britte L 2014 Comparison of torsional vibration measurement techniques *Advances in Condition Monitoring of Machinery in Non-Stationary Operations* eds G Dalpiaz *et al* (Berlin: Springer) pp 453–63
[27] Vishay Application of optical reflex sensors document number 80107, 02-02 (www.vishay.com/docs/80107/80107.pdf) (Last Accessed: 18 May 2017)
[28] Oppenheim A V, Schafer R W and Buck J R 1999 *Discrete-Time Signal Processing* (Upper Saddler River, NJ: Prentice Hall)
[29] ISO/IEC 2008 *Guide 98-3:2008 Uncertainty of Measurement—Part 3: Guide to the Expression of Uncertainty in Measurement (GUM:1995)* (International Organisation for Standardization)
[30] ISO/IEC 2008 *Guide 98-3:2008/Suppl.1:2008 Uncertainty of Measurement—Part 3: Guide to the Expression of Uncertainty in Measurement (GUM:1995)—Supplement 1: Propagation of Distributions using a Monte Carlo Method* (International Organisation for Standardization)
[31] UNI EN ISO 286-1 2010 *Geometrical Product Specifications (GPS)-ISO Code System for Tolerances on Linear Sizes—Part 1: Basis of Tolerances, Deviations and Fits* (International Organisation for Standardization)